Lumped chemical kinetic modelling of raw and torrefied biomass under pressurized pyrolysis

Saartjie Gouws, Marion Carrier, John Reginald Bunt, Hein W.J.P. Neomagus

Lumped chemical kinetic modelling of raw and torrefied biomass under pressurized pyrolysis

Saartjie M. Gouws [a], Marion Carrier [b], John R. Bunt [a,*], Hein W.J.P. Neomagus [a]

[a] Centre of Excellence in Carbon-based Fuels, School of Chemical and Minerals Engineering, North-West University, Potchefstroom, 2520, South Africa
[b] RAPSODEE, CNRS UMR 5203, Université de Toulouse, IMT Mines Albi, Campus Jarlard, 81013 Albi CT Cedex 09, France

Keywords:
Biomass
Torrefaction
Pyrolysis
Kinetics
Modelling
Pressurized pyrolysis

A B S T R A C T

Accurate prediction of the yield and composition of pyrolysis products is an important requirement for the design and operation of pyrolysis reactors and gasifiers. In this paper, a new semi-global kinetic reaction scheme is proposed to predict the composition of pyrolytic volatiles (classified as main chemical family groups), non-condensable gases and char derived from both raw and torrefied biomass for a wide range of operating conditions. The model is based on an adjustable mechanistic reaction scheme, which includes a combination of three different sub-mechanisms for the primary pyrolysis of three reference biopolymers (cellulose, hemicelluloses and lignin) and the secondary pyrolysis of their respective intermediates. The extent of primary/secondary reactions is varied according to the main process features (linear heating rate, temperature, pyrolysis time, volatile residence time and pressure). The secondary reactions in the scheme involve liquid-phase reactions of high molecular weight intermediates (producing non-condensable gases, water vapour and secondary char) as well as homogeneous and heterogeneous gas-phase conversion of primary volatiles. The model predictions were validated using experimental data obtained from fast pyrolysis in different micropyrolyzers (at 500–600 °C and heating rates of 27 and 110 °C/s, respectively) and slow pyrolysis in a laboratory-scale high-pressure fixed bed reactor (at 400–600 °C, 7 °C/min and 1, 15 and 30 bar). In general, the comparison of model outputs and experimental data were satisfactory, and the model predicted accurate trends in product distribution for changes of the lignocellulosic composition (the pre-removal of hemicelluloses in the case of torrefied biomass), heating rate and pressure. The model correctly predicted a significant increase in char yield (14.6 wt%) when torrefied instead of raw biomass was pyrolyzed due to the significance of char-forming reactions during pyrolysis of torrefied biomass. Moreover, the model's reliability was proven through its accurate prediction of various condensate groups in bio-oil produced in a micropyrolyzer (maximum deviation < 4 wt%). Corresponding to the experimental data, the model predictions showed that the effect of pressure was most significant in the range of 1–15 bar (bio-oil yield decreased by 5.4 wt%), whereas no significant effect in bio-oil yield was evident for a pressure increase in the range of 15–30 bar. The CO_2 and CO yields were slightly under-predicted by around 3 wt %, attributed to the catalytic effects of inherent inorganics on secondary cracking reactions which were not considered in the reaction scheme. Future work should focus on the validation of the model at temperatures below 400 °C.

1. Introduction

The global demand for energy and chemicals continues to rise and the world energy consumption is expected to increase a further 28% by 2040 [1]. These demands are accompanied by intensified calls for renewable energy and products to reduce greenhouse gas (GHG) emissions and limit climate change [2]. The pyrolysis process has received significant interest for its potential to co-generate both renewable energy and chemicals from biomass [3]. The pyrolysis liquid product derived during rapid heating of biomass, referred to as 'bio-oil', has been successfully used as boiler fuel and has also shown great promise for use in diesel engines [4]. Various chemicals such as polyols, alcohols, light olefins and aromatic hydrocarbons can also be produced from bio-oil [5]. Although bio-oil is promising for different applications, some of its properties limit its success. In particular, its high oxygen content (around 40% [5]) gives the oil an acidic nature, a low calorific value and a high chemical reactivity, resulting in phase separation during storage

* Corresponding author.
E-mail address: John.Bunt@nwu.ac.za (J.R. Bunt).

Nomenclature

ANN	Artificial Neural Network
ANN – GA	Artificial Neural Network tuned by genetic algorithm
ANN – PSO	Artificial Neural Network tuned by particle swarm optimization
Bio-CPD	Bio chemical percolation devolatilisation
Bio-FG-DVC	Bio functional group depolymerisation, vapourisation and cross-linking
d.a.f.	Dry ash free basis
d.b.	Dry basis
FID	Flame Ionization Detector
GC	Gas chromatography
HMWCs	High molecular weight components
LMWCs	Low molecular weight components
MAE	Mean absolute error
MS	Mass spectrometer
RAC	Ranzi and Anca-Couce model
r_j	Rate of primary reaction j
RMSE	Root mean square error
r_{sj}	Rate of secondary reaction j
SAPPI	South African Pulp and Paper Industries

[6]. Furthermore, depending on its polarity, some unrefined bio-oil is immiscible with hydrocarbon fuels [7].

One option for improving the chemical composition of bio-oil to closer resemble that of crude-oil by decreasing the oxygen content, is through thermal pre-treatment (torrefaction) of feedstocks [8]. Torrefaction is a mild type of thermal treatment performed at temperatures of 200 to 300 °C and has received significant interest due to its simplicity and economic feasibility [9]. During this process, moisture is removed, hemicelluloses are decomposed and lignin and cellulose are partially depolymerized [8]. The chemical and physical properties of the biomass as fuel are thereby improved: it has a lower O/C ratio, higher energy density and improved grindability [10,11]. The use of torrefied biomass as feedstock for pyrolysis also improves the composition of the produced bio-oil by reducing the moisture, oxygen and acid content, and increasing the carbon content [6].

To stimulate the commercialization of pyrolysis technologies, a reduction in process costs is required, which may be achieved through optimized design and operation of the process. To achieve this, effective and accurate modelling to predict final product composition is required. For this reason, kinetics and modelling of the pyrolysis process have a long history; however, it remains a complex field [12,13]. Xia et al. [14] and Perera et al. [15] have recently reviewed the state-of-the-art in modelling of biomass thermochemical conversion processes and demonstrated that three different types of modelling approaches are employed, including empirical, semi-empirical and fundamental analysis.

From those approaches, numerous biomass pyrolysis models are available with different advantages, limitations, and scale of applicability (Table 1). The most popular models are based on an irreversible single-step and endothermic reaction used to describe cellulose pyrolysis [16]. To further improve the predictability of those kinetic models and provide further reactional features, semi-global models (lumped models) were developed such as the multi-step reactional scheme of cellulose (Broido-Shafizadah [17]) and hemicelluloses (Di Blasi and Lanzetta [18]). Alternatively, global kinetic models with even more detailed degradation schemes were proposed by Mamleev et al. [19] and Rousset et al. [20]. Those detailed mechanistic models can become difficult to interpret physically and extrapolate, and may have a limited predictive capability [21], while judicious lumping models that still reflect the complexity of the reactant structures and the multiplicity of parallel and consecutive reactions, are probably more promising. Input/output modelling such as Monte Carlo and ANN (Artificial Neural Network), and network modelling such as the Bio-CPD (chemical percolation devolatilization), Bio-Flashchain and Bio-FG-DVC (functional group depolymerisation vaporization and cross-linking) models [22] are limited in terms of prediction and extrapolation [13], in particular for the yield and composition of bio-oil.

Ranzi et al. [23] proposed a semi-detailed mechanistic reaction scheme to describe both the complex nature of lignocellulose and competing reactional network taking place during biomass pyrolysis, suggesting the combination of different sub-mechanisms for the main biopolymers in biomass (cellulose, hemicelluloses and lignin). The main advantage of this scheme is that it is based on main pathways (although simplified) and it predicts the pyrolysis product yields taking into consideration the varying lignocellulosic composition of the biomass feedstock. The change in biomass composition during torrefaction with the removal of hemicelluloses may therefore be accounted for in the scheme. Furthermore, it provides detailed predictions of the oil and gas compositions.

The main limitations of the Ranzi scheme are that it does not include secondary charring and cracking reactions, nor the formation of high molecular weight components, such as oligomers. Moreover, the ability of the scheme to predict the product yields and composition of high pressure pyrolysis (the first step in the commercial fixed bed dry bottom gasifier (FBDB^{TM}) [24]), was not assessed. Anca-Couce et al. [25] adapted the original scheme of Ranzi et al. [26] (RAC model) to account for secondary charring reactions by introducing an adjustable parameter "x" to vary the amount of initial fragmentation products. The authors suggested that this parameter would be affected by pressure but did not test their hypothesis. Although this model shows improved predictions for the pyrolysis product yields at low pressures, a disadvantage is that the "x" parameter is not based on an explicit understanding of the physics and therefore it is unlikely that the model can be extrapolated.

In addition to capturing relevant degradation trends, the semi-global models may also be adapted to heating conditions and related to pyrolysis modes such as slow and fast pyrolysis. Pyrolysis is generally performed at temperatures of 500–600 °C, where slow pyrolysis targets the char product, while fast pyrolysis targets the bio-oil/condensate product through short volatile residence times (<6 s) [27]. The low heating rates (<10 °C/min) used during slow pyrolysis allow the weakest chemical bonds to break first whilst the stronger bonds remain stable, favouring recombination/charring reactions; whereas the high heating rates (>100 °C/s) used in fast pyrolysis results in the simultaneous breakage of various bonds, releasing high amounts of volatile compounds before recombination/charring reactions can occur [28]. Moreover, during slow pyrolysis the heating period is sufficiently low for the reactions to reach equilibrium, but this is not the case during fast pyrolysis [29]. The vapour residence time, pressure and time–temperature history to which the primary volatiles are subjected also plays a significant role in the extent of homogeneous and heterogeneous secondary reactions (and therefore product yield and composition) [30,31]. Semi-global models therefore need to be adapted by keeping in mind the reactor configuration and operating conditions.

An important requirement for accurate and robust model development is that a suitable reactor design should be used, and reliable experimental data obtained for validation purposes. Analytical pyrolysis is the method of choice as it allows the monitoring and identification of hot pyrolytic volatiles released over time as well as screening the thermal behaviour of a wide range of biomasses [32]. With regard to torrefied biomass, a few analytical pyrolysis (using Py-GC–MS) studies have demonstrated how changes in biopolymer composition, due to torrefaction, altered the composition of volatiles. Neupane et al. [33] reported that torrefaction pre-treatment of biomass resulted in an increase in aromatic hydrocarbons and phenolic groups and a decrease in furan groups and Cai et al. [34] similarly reported an enriched content of phenolic groups in bio-oil derived from pre-torrefied wood. Chen et al.

Table 1
Comparison of advantages, limitations and scale of applicability of existing pyrolysis models and the new lumped kinetic model.

Model	Modelling approach	Model type	Advantages	Limitations	Scale of applicability	Ref.
Monte Carlo	Empirical	Input/ output	Accurate predictions of complex input/output relationships. Short simulation time.	Only applicable for reactor/fuels for which it was developed.	Laboratory scale/commercial.	[39]
ANN	Empirical	Input/ output	Accurate predictions of char yields. Moderate computation ability required.	Only applicable for reactor/fuels for which it was developed. Large number of experimental data is required for tuning.	Laboratory scale/commercial.	[40]
ANFIS – PSO and ANFIS – GA	Semi-empirical	Input/ output	Reliable and robust predictions. Applicable to different types of biomass (considers lignocellulosic composition/ultimate analysis)	Large number of experimental data is required for tuning. Loss of fundamental meaning of kinetic parameters. Only applicable for reactor for which it was developed	Laboratory scale/commercial.	[41,42]
Bio-CPD	Semi-empirical	Input/ output	Applicable to different types of biomass (considers feedstock proximate/ultimate analysis). Accurate predictions of main pyrolysis product yields.	Limited extrapolation capability. Cannot predict bio-oil composition. Originally based on coal's structure.	Laboratory scale/commercial.	[43]
Bio-Flashchain	Semi-empirical	Input/ output	Applicable to different types of biomass (considers feedstock proximate/ultimate analysis). Accurate predictions of product elemental composition.	Limited extrapolation capability (model not valid for slow pyrolysis). Cannot predict bio-oil composition.	Laboratory scale/commercial.	[44]
Bio-FG-DVC	Semi-empirical	Input/ output	Accurate prediction of pyrolysis gas composition and char yields.	Only applicable for fuels and conditions for which it was developed. Cannot predict bio-oil composition.	Laboratory scale/commercial.	[45]
One-step reaction	Semi-empirical	Semi-global	Low computation ability is required.	Cannot be extrapolated to different reactors and heating rates. Low accuracy.	Laboratory scale (primary pyrolysis conditions).	[16]
Broido-Shafizadah	Fundamental analysis	Semi-global	Based on fundamental reaction pathways. Low computational capability is required due to lumping of products.	Secondary reactions are not described. Effect of volatile residence time, pressure and inherent inorganics on product yields is not considered.	Laboratory scale (primary pyrolysis conditions) .	[17]
Di Blasi and Lanzetta	Fundamental analysis	Semi-global	Reaction scheme is based on experimental observations. Low computational capability is required due to lumping of products.	Secondary reactions not described. Effect of volatile residence time, pressure and inherent inorganics on product yields is not considered	Laboratory scale (primary pyrolysis conditions).	[18]
Ranzi and RAC	Fundamental analysis	Semi-global	Detailed description of pyrolysis products based on main reaction pathways. Applicable to different types of biomass (considers lignocellulosic composition).	Secondary cracking reactions are not described. Formation of HMWCs/oligomers is not considered. Effect of volatile residence time, and pressure is not considered.	Laboratory scale (primary pyrolysis conditions).	[26 25]
Rousset	Fundamental analysis	Global	Detailed description of fundamental chemistry. Applicable to both micro- and macroscale pyrolysis.	Requires large computational capacity. Effect of volatile residence time, pressure and inherent inorganics is not considered. Difficult to interpret physically and extrapolate.	Laboratory/commercial scale.	[20]
Mamleev	Fundamental analysis	Global	Detailed description of fundamental chemistry. Transformation processes inside the cellulose matrix are considered.	Limited to cellulose pyrolysis. Large computational capacity is required. Secondary reactions are not described. Difficult to interpret physically and extrapolate.	Laboratory scale (primary pyrolysis conditions).	[19]
New Lumped kinetic model	Fundamental analysis	Semi-global	Based on fundamental reaction pathways. Secondary charring/cracking reactions are included. The formation of HMWCs/oligomers is included. The effect of pressure on pyrolysis product yields is considered. Reaction scheme is adapted according to process conditions.	Catalytic effect of inherent inorganics is not considered. Interactions between biomass components are not considered. Lack of precise kinetic parameters for secondary reactions. Requires validation for commercial scale reactors.	Laboratory/commercial scale (considers both primary and secondary reactions).	

[35] qualitatively observed a decrease in furan groups and an increase in levoglucosan in bio-oil after torrefaction. The decrease in the selectivity of furan groups was directly correlated with the reduced hemicelluloses content of the material, which demonstrates that biopolymer composition of torrefied biomass should be an important modelling input parameter [34,36,37]. Although the use of those analytical pyrolysis techniques have increased in popularity, the accurate quantification of GC-detected components remains a challenge [38] and great efforts have been dedicated to developing a reliable quantification methodology.

In this paper, a new semi-global kinetic model including an adjustable mechanistic pyrolysis reactional scheme (varying the lignocellulosic composition and the primary/secondary reactions presence with the setting of the main process features of the process i.e. linear heating rate, temperature, pyrolysis time, volatile residence time and pressure) was developed to predict the composition of the pyrolytic volatiles classified as main chemical family groups, non-condensable gases and char produced from raw/torrefied biomass. To do this, the primary reactional scheme was first established from both the characterization of hot volatiles and condensates obtained under fast pyrolysis conditions using two different micropyrolyzers: (1) a μg-scale micropyrolyzer (Multi-shot pyrolyzer) with micro-furnace system and (2) a mg-scale micropyrolyser (Horizontal micropyrolyzer). The secondary reactional scheme was assessed based on the bio-oil characterisation of pressurized biomass slow pyrolysis. The main advantages and novelties of this new model is that it considers the formation of high molecular weight components (HMWCs), the presence of secondary charring and cracking reactions as well as the effect of pressure on these reactions (Table 1). Moreover, the model is applicable to various scales of pyrolysis due to the adjustable nature of the reaction scheme corresponding to the main process characteristics of different reactors.

2. Material and methods

2.1. Raw and torrefied materials

The experimental pyrolysis product data, which was used to validate the model predictions, was obtained from different woody biomasses. This included raw and torrefied wood (mixture of soft and hardwood species from South Africa) chips as well as raw pine (*Pinus radiata* from Chile) sawdust. Both preparation and characterization of feedstocks, raw/torrefied woods and pine sawdust, were respectively reported by Gouws et al. [31] and Moore et al. [46]. A summary of the proximate and ultimate analyses of the different woody biomass samples is shown in Table 2, whereas the compositional analysis (required as input parameters to the model) is provided in Table 3.

2.2. Pyrolysis reactors

Three different pyrolysis reactors (Fig. 1) were considered where the pyrolysis process was conducted on 3 different scales: (1) a μg-scale micropyrolyzer (Multi-shot pyrolyzer) with micro-furnace system (details in Section 2.3.1), (2) a mg-scale micropyrolyser (Horizontal micropyrolyzer) (details in Carrier et al. [47]) and (3) a g-scale high-pressure pyrolyzer (details in Gouws et al. [31]). Further details on the dimensions and operating conditions of these reactors are provided in Table 8.

Table 2
Proximate and ultimate analyses of different woody biomass samples adapted from Moore et al. [46] and Gouws et al. [31].

	Standard method	Raw wood chips	Torrefied wood chips	Pine sawdust
Proximate analysis in wt.% (d.b.[a])				
Volatile matter	ISO 562:2010	82.9	70.4	94.7
Ash	ISO 1171:2010	1.5	2.0	0.92
Fixed carbon	by difference	15.6	27.5	4.38
Ultimate analysis in wt.% (d.a.f.[b])				
Carbon	ASTM D5373	54.4	59.5	46.5
Hydrogen	ASTM D5373	5.8	5.7	5.4
Nitrogen	ASTM D5373	0.1	0.1	0.1
Sulfur	ASTM D4239	0.1	0.1	n.r.
Oxygen	by difference	39.6	34.7	48.0

[a]d.b. – dry basis, [b]d.a.f. – dry ash free basis, n.r. – not reported.

2.3. Condensables and condensates characterisation

2.3.1. Condensable (hot volatiles) analysis

Analytical pyrolysis experiments were performed in a multi-shot pyrolyzer (EGA/PY-3030D) coupled to a gas chromatograph (Agilent 8890) mass spectrometer (Agilent 5977) and FID detector. The sample (~0.2 mg) was loaded into a stainless steel cup (coated with a thin quartz film) which was then attached to a sample holder with a quartz coated steel stick. A volume of 2 μL internal standard solution (25 mg/mL of Fluoranthene (Purity 98%, Sigma-Aldrich)) in acetone (SupraSolv for ECD and GC-FID, Sigma-Aldrich) was dropped on quartz wool placed above the solid sample to act as an internal standard. Subsequently, both the sample holder and cup were introduced into the pyrolyzer and 1 min waiting time was allowed to purge the dead space at the sample/furnace coupling. Thereafter, the cup was dropped into the pre-heated furnace at the desired temperature (500, 550 and 600 °C). The heating rate applied was calculated to be 110 °C/s in this reactor (see Section 3.2) and the interface between the furnace and the GC injection port was maintained at 280 °C. The released volatiles were injected using a split ratio of 50:1 at 280 °C and subsequently separated and analysed via the GC–MS/FID system. This latter was equipped with a HP-5MS capillary column (30 m × 250 μm × 0.25 μm). The pyrolysis was conducted using Helium (Scientific grade 6.0, Linde France) at a flow rate of 54 mL/min. The details of the GC–MS/FID system are summarized in Table 4.

Quantification of 15 major components was performed according to a novel internal calibration method described here. First, a solution of 25 mg/mL of Fluoranthene (98%, Sigma-Aldrich) in acetone was prepared as internal standard. Multi-standard solutions provided by Restek were used and calibration solutions were prepared by adding 50, 125, 250, 375 and 490 μL of each multi-standard solution respectively to 440, 365, 240, 115 and 10 μL of acetone, which resulted into 5 standard solutions. Calibration samples were prepared by adding 10 μL of the internal standard solution into 500 mL of the standard solutions. In parallel, additional standard solutions for hydroxyacetone, furfural, 5-HMF and levoglucosan were prepared. A volume of 2 μL was dropped on glass wool placed into the cup and exposed to an equivalent operating environment and chromatographic conditions to that of the experiments. A series of calibration curves was obtained and are displayed in the Supplementary Data (Section S1). By using this technique, any chemical changes of the sample were avoided and effective devolatilization of the internal standard was obtained.

An evolved gas analysis was performed to determine the reaction time of the raw and torrefied biomass samples during pyrolysis. The same pyrolysis conditions and parameter settings were maintained, only the column was changed to an Ultra Alloy deactivated and uncoated stainless-steel capillary tube (Length: 2.5 m; ID: 150 μm and OD: 470 μm, Frontier Lab) kept at 300 °C. The inertness of the glass quartz wool as well as the absence of mass transfer limitations was verified (Supplementary Data Section S2). The carrier gas flow was set at 50 L/min. The gas evolution curves are shown in the Supplementary Data (Section S3) and from these results the reaction time was determined to be 1.2 min for raw biomass and 1.5 min for torrefied biomass.

2.3.2. Condensates (bio-oil) analyses

The identification and quantification of the condensates derived from the pine sawdust in the mg-scale micropyrolyser (Horizontal micropyrolyzer) was performed using a gas chromatograph (HP 6890 Agilent) system coupled to a mass spectrometer (HP 5972). The GC was equipped with a Varian VF 1701-MS column (14% cyanopropylphenyl/methylpolysiloxane, 60 m × 0.25 mm × 0.25 mm). Full details of the analysis method are reported in Carrier et al. [47].

The analysis of the condensates derived from the torrefied biomass in the g-scale high-pressure pyrolyser was performed on a gas

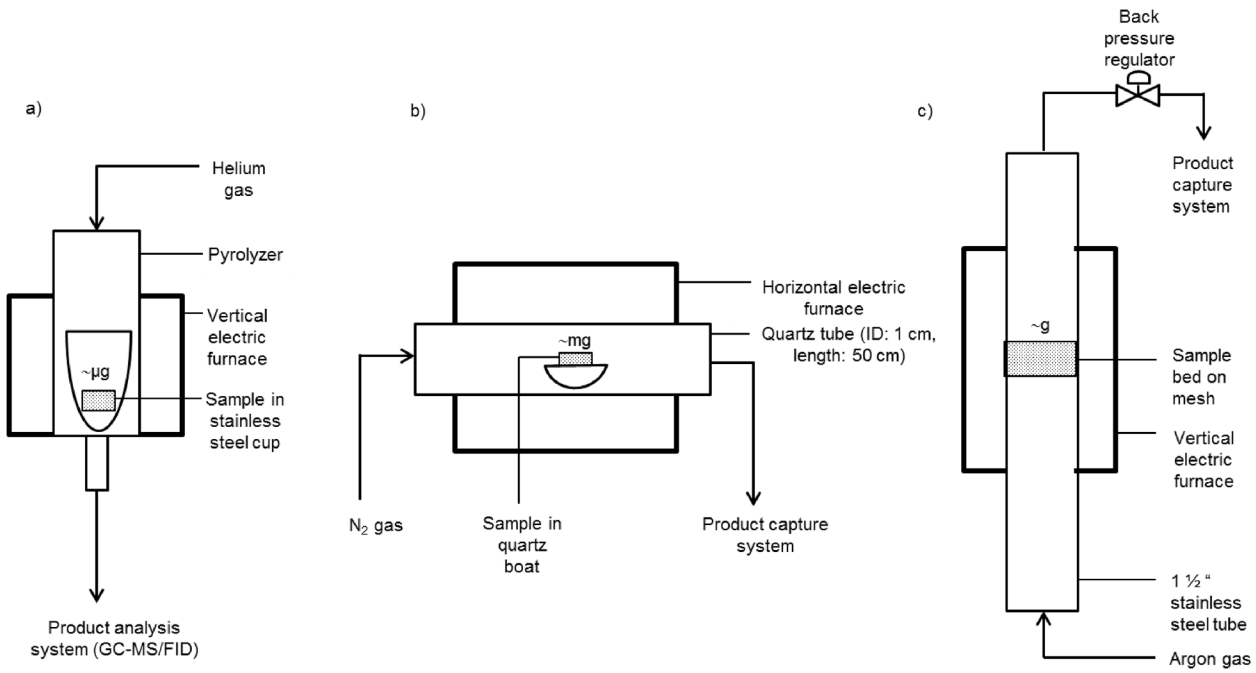

Fig. 1. Reactor configuration of a) µg-scale micropyrolyzer (Multi-shot pyrolyzer), b) mg-scale micropyrolyser (Horizontal micropyrolyzer) and c) g-scale high-pressure pyrolyzer.

Table 3
Compositional analysis of different woody biomass samples in wt.% (d.a.f.) adapted from Moore et al. [46] and Gouws et al. [31].

	Raw wood chips	Torrefied wood chips	Pine sawdust
Hemicelluloses	12.4	1.4	4.4
Cellulose	61.1	61.5	54.5
Lignin	26.5	37.1	41.2

Table 4
GC–MS/FID parameter details.

Parameter	Details
GC carrier gas and flow rate	Helium, 1 mL/min
GC oven temperature program	Stage 1: 50 °C for 2 min Stage 2: 50 – 200 °C at 2 °C/min , hold 2 minStage 3: 200 – 320 °C at 10 °C/min
MS operation mode	Electron impact (EI), Scan from 29 to 350 *m/z*
MS ionization energy	70 eV
Identification software	NIST 17 library
Source temperature	230 °C
Quadrupole temperature	150 °C
Transfer line temperature	250 °C
FID operation temperature	300 °C
FID gases and flow rates	Hydrogen, 30 mL/min Air, 300 mL/min

chromatograph (6890 N, Agilent technologies network) coupled to an Agilent technologies inert XL EI/CI Mass Selective Detector (MSD) (5975B, Agilent technologies). A ZB-Waxplus capillary column (30 m × 0.25 mm × 0.25 µm) from Phenomenex was used for the GC column. Full details of the analysis method are reported in Gouws et al. [31].

3. Pyrolysis kinetic model development

In this section, the development of the lumped chemical kinetic model is presented (Section 3.1), followed by the determination of the main process characteristics for the different pyrolysis reactors (Section 3.2). The development of the reaction kinetic model (Section 3.1) includes the derivation of the primary and secondary reaction schemes (Section 3.1.1) as well as the kinetic data (Section 3.1.2). Furthermore, the effect of the reactor temperature and time history (Section 3.2.1) and the volatile residence time and pressure (Section 3.2.2) on the adjustable reaction scheme is discussed.

3.1. Reaction kinetic model

3.1.1. Primary and secondary reaction schemes

The kinetic approach is based on a well-proven semi-global methodology [23,48] for which the apparent reaction model for biomass pyrolysis is described as the combination of three different sub-mechanisms for the pyrolysis of three reference biopolymers (cellulose, hemicelluloses and lignin) (Fig. 2), for which the fractional mass was determined from a compositional analysis (Table 3). The three independent multistep kinetic models are described as a series of consecutive first order reactions (rate equations are shown in the Supplementary Data (Section S4)). The volatile products are grouped into main chemical families: acids, alcohols, aldehydes, furanics, ketones, sugars, methoxyphenols and phenols. During pyrolysis, each biopolymer is first converted into two intermediate pseudo-components: Low molecular weight components (LMWCs) (reactions 1, 6, 10) and high molecular weight components (HMWCs) (reactions 2, 7, 11) based on the general understanding that biomass forms a liquid-phase intermediate component during pyrolysis, which then reacts further via different competing reactions [49,50].

For cellulose, a charring reaction (reaction 3), which produces primary char and water, competes with the reactions forming the intermediate components (reactions 1 and 2) as originally suggested in the scheme by Piskorz et al. [51]. Reactions 1 and 2 are the dominant reactions for the conversion of cellulose but reaction 3 becomes more significant at lower temperatures (due to the lower activation energy). From the cellulose-derived intermediate LMWCs ($LMWC_{CELL}$), transglycosylation (reaction 4) and fragmentation (reaction 5) pathways compete and produce sugars and low molecular weight volatiles (aldehydes, furanics, ketones, acids and non-condensable gases), respectfully.

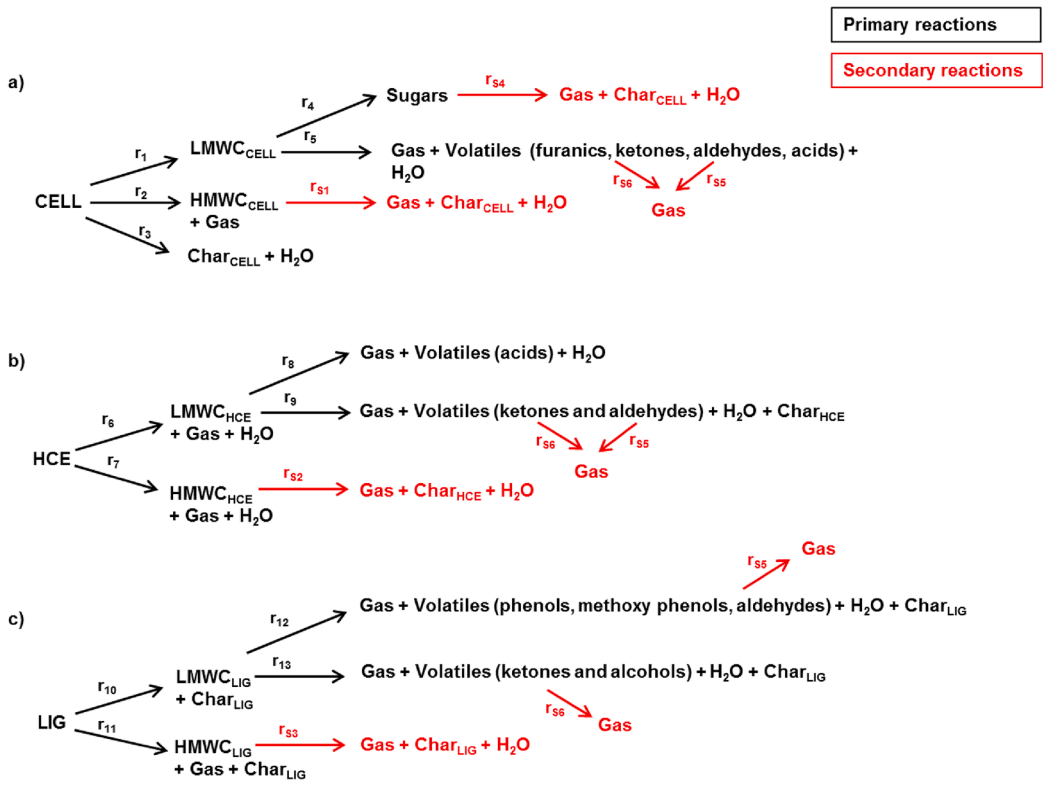

Fig. 2. Reactional kinetic scheme for pyrolysis of a) cellulose (CELL), b) hemicelluloses (HCE) and c) lignin (LIG).

For the hemicelluloses, the LMWCs (LMWC$_{HCE}$) decompose via two different pathways: fragmentation (reaction 8), which is the dominant pathway where low molecular weight volatiles, including short-chained acids and non-condensable gases are produced [52], and a char-forming pathway (reaction 9), which becomes more significant at lower temperatures. The lignin-derived LMWCs (LMWC$_{LIG}$) react via competing phenolic-formation (reaction 12) and fragmentation (reaction 13) pathways [26], which produce phenols and methoxyphenols, and light volatiles (aldehydes, ketones and non-condensable gases), respectfully.

The HMWCs represent the anhydro-oligosaccharides derived from cellulose (HMWC$_{CELL}$) and hemicelluloses (HMWC$_{HCE}$) and the oligomers derived from lignin (HMWC$_{LIG}$). To our knowledge, the formation of these HMWCs has not been included in previous semi-global models. If not rapidly evaporated, removed and condensed, these HMWCs undergo secondary reactions in the molten intermediate phase (reactions S1-S3) to produce char, water and non-condensable gases [53]; therefore, the addition of these secondary reactions to the reaction scheme depends on the pyrolysis operating conditions (further details in Section 3.2.2). Furthermore, the reaction scheme also accounts for gas-phase secondary reaction pathways of major primary volatiles (reactions S4-S6), the extent of which is affected by process characteristics (Section 3.2.2). These pathways include homogeneous (cracking) of low molecular weight groups (aldehydes and ketones) (reactions S5-S6), producing non-condensable gases and heterogeneous (charring) of primary sugars (reaction S4), producing char, water and non-condensable gases.

The molecular formula (Table 5) of the most abundant components in each volatile chemical group was assumed to be representative for the chemical family, whereas the molecular formulas of the intermediate LMWCs derived from the different biopolymers (LMWC$_{CELL}$, LMWC$_{HCE}$, LMWC$_{LIG}$) was determined by assuming it to be equal to the average molecular weight of GC-detectable components in bio-oil produced from the different biopolymers. A comprehensive quantitative GC–MS/FID analysis of bio-oil derived from cellulose, hemicelluloses and lignin, respectively, (reported by Carrier et al. [47]) was used for this purpose. In their analysis, 98.0% of the GC peak areas from cellulose-derived oil, 90.7% of the GC peak areas from hemicelluloses-derived oil, and 91.0% of the GC peak areas from lignin-derived oil were quantified, which allowed a reliable estimate of the molecular weights of the LMWCs derived from each biopolymer.

For the HMWCs components (HMWC$_{CELL}$, HMWC$_{HCE}$, HMWC$_{LIG}$), the molecular formulas were obtained from the study by Xiong et al. [54]. They used a Fourier transform ion cyclotron resonance mass spectrometer (FT-ICR-MS) and an ultraviolet fluorescence (UV-F) spectrometer to determine molecular formulas of heavy components in bio-oil derived from cellulose, hemicelluloses and lignin. Furthermore, the molecular formulas of the chars (Char$_{CELL}$, Char$_{HCE}$, Char$_{LIG}$) were estimated from the elemental analysis of chars derived from cellulose, hemicelluloses and lignin at temperatures of 400–600 °C, reported by Smith et al. [55]. The reaction stoichiometry for the primary and secondary reactions were obtained from literature [23,56,57], although slight adjustments were necessary to balance the equations in some cases. The detailed reaction scheme for the primary reactions and secondary reactions is shown in Tables 6 and 7, respectively.

3.1.2. *Kinetic data*

The kinetic triplets reported in the reaction scheme by Ranzi et al. [23] were used to model reactions 1–13 for raw biomass (Table 6) and it was assumed that the reactions producing the intermediate components (LMWCs and HMWCs) have similar rates. The kinetic triplets for these reactions (reactions 1, 2, 6, 7, 10 and 11) were obtained from the reactions forming intermediate components in the scheme of Ranzi et al. [23] (reactions 2, 5 and 10 in their scheme). For torrefied biomass, the kinetic triplets reported by Wang et al. [58] (Table 6) were used for the char-forming reactions (reactions 3, 10, 11 and 12) (further details in Section 4.1).

The kinetic parameters for the liquid-phase secondary reactions of HMWC$_{CELL}$ (reaction S1) and HMWC$_{HCE}$ (reaction S2) were obtained from Di Blasi [59] (Table 7), whereas for the reaction of HMWC$_{LIG}$ (reaction S3), the kinetic triplet reported by Branca et al. [60] for the devolatilization of the heavy fraction of bio-oil (consisting mainly of

Table 5
List of species and their molecular formula/weight.

Abbreviation	Description	Molecular formula	Molecular weight (g/mol)
Reagents			
CELL	Cellulose	$C_6H_{10}O_5$	162.1
HCE	Hemicelluloses	$C_5H_8O_4$	132.1
LIG	Lignin	$C_{15}H_{14}O_4$	258.1
Products			
Volatiles			
Sugars	Sugars	$C_6H_{10}O_5$	162.1
Aldehydes	Aldehydes	$C_2H_4O_2$	60.0
Furanics	Furanics	$C_5H_4O_2$	96.0
Ketones	Ketones	$C_3H_6O_2$	74.1
Acids	Acids	$C_2H_4O_2$	60.0
Methoxyphenols	Methoxyphenols	$C_9H_{12}O_2$	152.1
Phenol	Phenol	C_6H_6O	94.1
Alcohols	Alcohols	CH_4O	32.0
Solid products			
$Char_{CELL}$	Char derived from cellulose	$C_{25}H_9O$	325.1
$Char_{HCE}$	Char derived from hemicelluloses	$C_{22}H_4O$	284.0
$Char_{LIG}$	Char derived from lignin	$C_{21}H_4O$	272.0
Gas products			
H_2O	Pyrolytic water	H_2O	18.0
CO	Carbon monoxide	CO	28.0
CO_2	Carbon dioxide	CO_2	44.0
CH_4	Methane	CH_4	16.0
H_2	Hydrogen	H_2	2.0
Intermediate products			
$LMWC_{CELL}$	Low molecular weight components from cellulose	$C_5H_8O_4$	132.1
$HMWC_{CELL}$	High molecular weight components from cellulose	$C_{18}H_{24}O_8$	368.2
$LMWC_{HCE}$	Low molecular weight components from hemicelluloses	$C_3H_5O_2$	73.1
$HMWC_{HCE}$	High molecular weight components from hemicelluloses	$C_{19}H_{22}O_8$	378.2
$LMWC_{LIG}$	Low molecular weight components from lignin	$C_5H_7O_2$	99.1
$HMWC_{LIG}$	High molecular weight components from lignin	$C_{26}H_{40}O_4$	416.4

lignin-derived high molecular weight components) was used. For the gas-phase secondary reactions, the kinetic triplets reported by Di Blasi [59] was used for the heterogeneous (charring) reaction (reaction S4), whereas those reported by from Park et al. [61] where used for the homogeneous (cracking) reactions (reactions S5-S6) (Table 7).

3.2. Determination of main process characteristics

3.2.1. Temperature and time history

As kinetically controlled isothermal pyrolysis is rarely achieved, thermal profiles, here linear heating ramps (Table 8) corresponding to the heat-up phase of the particles for each experimental reactor system, were considered. Detailed calculations are shown in the Supplementary Data (Section S5) and further details on the operating conditions of the pyrolysis reactors are shown in Table 8.

The effect of time is related to the role of the heating rate, and therefore to the type of reactor used. From Table 8, it is clear that in this study extremes were considered: on one hand, in the fixed-bed reactor, the time effect is not as important because the time it takes to reach the final pyrolysis temperature is much longer than that needed to complete the pyrolysis reactions; on the other hand, in the multi-shot reactor, the time is shorter, and its influence remains significant.

Table 6
Detailed reaction scheme of primary reactions for raw/torrefied biomass and their kinetic parameters for a temperature range of 400–600 °C.

	Primary reaction	Kinetic parameters for raw biomass [23]		Kinetic parameters for torrefied biomass [23,58]	
		A (s^{-1})	E (kJ/mol)	A (s^{-1})	E (kJ/mol)
1	CELL ($C_6H_{10}O_5$) → 1.24 $LMWC_{CELL}$ ($C_5H_8O_4$)	1.5 x10^{14}	196.6	1.5 x10^{14}	196.6
2	CELL ($C_6H_{10}O_5$) → 0.28 $HMWC_{CELL}$ ($C_{18}H_{24}O_8$) + 0.26 CO_2 + 0.63 CO + 1.59 H_2O	1.5 x10^{14}	196.6	1.5 x10^{14}	196.6
3	CELL ($C_6H_{10}O_5$) → 0.24 $Char_{CELL}$ ($C_{25}H_9O$) + 4.1 H_2O	6.0 × 10^7	129.7	1.3 × 10^{13}	183.2
4	$LMWC_{CELL}$ ($C_5H_8O_4$) → 0.81 Sugars ($C_6H_{10}O_5$)	3.3 × T	41.8	3.3 × T	41.8
5	$LMWC_{CELL}$ ($C_5H_8O_4$) → 0.46 Aldehydes ($C_2H_4O_2$) + 0.18 Furanics ($C_5H_4O_2$) + 0.40 Ketones ($C_3H_6O_2$) + 0.05 Acids ($C_2H_4O_2$) + 0.41 CO + 0.16 CO_2 + 0.05 H_2 + 1.03 H_2O + 0.05 CH_4 + 0.05 Char ($C_{25}H_9O$)	2.5 × 10^6	79.9	2.5 × 10^6	79.9
6	HCE ($C_5H_{10}O_5$) → 1.54 $LMWC_{HCE}$ ($C_3H_5O_2$) + 0.38 CO_2 + 0.15 H_2O	1.0 × 10^{10}	129.7	1.0 × 10^{10}	129.7
7	HCE ($C_5H_{10}O_5$) → 0.24 $HMWC_{HCE}$ ($C_{19}H_{22}O_8$) + 0.37 CO_2 + 1.32 H_2O	1.0 × 10^{10}	129.7	1.0 × 10^{10}	129.7
8	$LMWC_{HCE}$ ($C_3H_5O_2$) → 1.06 Acids ($C_2H_4O_2$) + 0.81 H_2O + 0.38 H_2 + 0.38 CO	3.0 × T	46.0	3.0 × T	46.0
9	$LMWC_{HCE}$ ($C_3H_5O_2$) → 0.03 H_2O + 0.05 CO_2 + 0.39 Ketones ($C_3H_6O_2$) + 0.24 CO + 0.16 H_2 + 0.40 Aldehydes ($C_2H_4O_2$) + 0.13 CH_4 + 0.03 $Char_{HCE}$ ($C_{22}H_4O$)	1.8 × 10^{-3} T	12.5	1.8 × 10^{-3} T	12.5
10	LIG ($C_{15}H_{14}O_4$) → 1.84 $LMWC_{LIG}$ ($C_5H_7O_2$) + 0.28 $Char_{LIG}$ ($C_{21}H_4O$)	1.0 × 10^{11}	155.6	1.0 × 10^{15}	211.6
11	LIG ($C_{15}H_{14}O_4$) → 0.32 $HMWC_{LIG}$ ($C_{26}H_{40}O_4$) + 1.22 CO_2 + 0.25 $Char_{LIG}$ ($C_{21}H_4O$)	1.0 × 10^{11}	155.6	1.0 × 10^{15}	211.6
12	$LMWC_{LIG}$ ($C_5H_7O_2$) → 0.19 Methoxyphenols ($C_9H_{12}O_2$) + 0.18 Phenol (C_6H_6O) + 0.30 Aldehydes ($C_2H_4O_2$) + 0.30 H_2O + 0.54 CH_4 + 0.10 H_2 + 0.47 CO + 0.05 $Char_{LIG}$ ($C_{21}H_4O$)	1.0 × 10^{11}	155.6	1.0 × 10^{15}	211.6
13	$LMWC_{LIG}$ ($C_5H_7O_2$) → 0.42 H_2 + 0.25 H_2O + 0.18 Aldehydes ($C_2H_4O_2$) + 0.49 CO + 0.38 Alcohols (CH_4O) + 0.19 Ketones ($C_3H_6O_2$) + 0.43 CH_4 + 0.13 $Char_{LIG}$ ($C_{21}H_4O$)	1.2 × 10^9	125.5	1.2 × 10^9	125.5

3.2.2. Volatile residence time and pressure

The extent of secondary reactions is known to depend on operating conditions as well as the reactor configuration [62–65]. Here, the volatile residence time and reactor pressure are considered as the process variables that primarily affect the secondary reactions and determine the fate of intermediate decomposition products. During fast pyrolysis in the multi-shot and horizontal microplyrolyzers, a short vapour residence time and low pressure were used; therefore, it is assumed that the rapid removal of the reactive intermediate HMWCs prevented subsequent liquid-phase secondary reactions (reactions S1-S3). Furthermore, it was also assumed that no gas-phase secondary reactions (reactions S4-S6) occurred in these reactors.

In contrast, during slow pyrolysis in the high-pressure pyrolyzer, the long vapour residence time (19.1 s) and high reactor pressures (15 and 30 bar) resulted in both liquid-phase and gas-phase secondary reactions, which was evidenced by the detection of a large number of secondary products [31]. Therefore, successive secondary liquid- and gas-phase

Table 7
Detailed reaction scheme of secondary reactions and their kinetic parameters for a temperature range of 400–600 °C.

	Secondary reaction	Kinetic parameters A_1 (s^{-1})	E_1 (kJ/mol)	Ref.
	Liquid-phase			
S1	$HMWC_{CELL}$ ($C_{18}H_{24}O_8$) → 0.57 Char ($C_{25}H_9O$) + 3.17 CO_2 + 9.43 H_2	4.48 × 10^6	106	[59]
S2	$HMWC_{HEC}$ ($C_{19}H_{22}O_8$) → 0.70 Char ($C_{22}H_4O$) + 3.7 CO_2 + 9.6 H_2	4.48 × 10^6	106	[59]
S3	$HMWC_{LIG}$ ($C_{26}H_{40}O_4$) → 0.77 Char ($C_{21}H_4O$) + 2.1 H_2 + 1.61 CO_2 + 8.18 CH_4	3.3 × 10^5	91	[60]
	Gas-phase			
S4	Sugars ($C_6H_{10}O_5$) → 0.22 Char ($C_{25}H_9O$) + 0.18 CO_2 + 4.02 H_2O + 0.40 CO	4.48 × 10^6	106	[59]
S5	Aldehydes ($C_2H_4O_2$) → 2.0 CO_2 + 2.0 H_2	4.28 × 10^5	108	[61]
S6	Ketones ($C_3H_6O_2$) → 0.5 CO_2 + 0.5 H_2 + 1.25 C_2H_4	4.28 × 10^5	108	[61]

reactions (reactions S1-S6) were considered in the reaction scheme for this reactor. The pressure was assumed to mainly affect the gas-phase homogeneous and heterogeneous secondary reactions and its influence was incorporated into the model through the assumption that the partial pressure of the primary volatiles could be directly determined from the reactor pressure via Equation 1 [65]:

$$p_j = x_j P \quad (1)$$

where x_j is the mole fraction of a primary volatile and P is the reactor pressure.

The rates of the secondary gas-phase reactions (reactions S5-S6) were therefore considered to be a function of the primary volatiles' partial pressure. Moreover, the rate of the heterogeneous secondary reaction (reaction S4) was also considered a function of the primary volatile partial pressure to account for the first-order effect of pressure on the adsorption of the primary volatiles onto the solid as suggested by Jones et al. [66]. In contrast, secondary reactions S1-S3 occurred in the liquid-phase, consequently their rates were assumed to be unaffected by the reactor pressure. The rate equations for the various secondary reactions are shown in the Supplementary Data (Section S4).

3.3. Model implementation

To model the pyrolysis process at different heating rates, the mass balances and reaction equations, coupled with the time–temperature equation, were numerically solved using Polymath Professional 6.0 Software. The initial masses of the cellulose, hemicelluloses and lignin were determined from the compositional analysis of the feedstock (Table 3). A 0D model was used with the code containing 26 first-order ordinary differential equations (ODE's), 44 explicit algebraic equations for the multi-shot and horizontal micropyrolyzer models and 69 explicit algebraic equations for the high-pressure pyrolyzer model. Integration over time was performed using the built-in Runge-Kutta-Fehlberg (RKF45) algorithm. The code is provided in the Supplementary Data (Section S6). The accuracy of the model was assessed through a statistical analysis by determining the root mean square error (RMSE) and mean absolute error (MAE) for the primary and secondary reaction schemes at different operating conditions.

4. Results and discussion

The validation of the primary and secondary reaction scheme is presented in this section. First, the primary scheme is validated by comparing the model outputs with experimental data derived from raw and torrefied biomass in the μg-scale micropyrolyzer (Section 4.1). Thereafter, the primary scheme is further validated using experimental data derived for pine sawdust in the mg-scale micropyrolyzer (Section 4.2). The secondary scheme is then validated by comparing the model outputs to the experimental data derived from torrefied biomass in the g-scale fixed bed pyrolyzer for both low (Section 4.3) and high (Section 4.4) pressures.

4.1. Model predictions and validation of primary condensables composition

The outputs of the multi-component kinetic model, the detailed characterization of released pyrolysis products, are discussed here based on a comparison between the model predictions and experimental results for the pyrolysis of raw (Table 9) and torrefied biomass (Table 10) at temperatures of 500–600 °C. When using the kinetic parameters reported by Ranzi et al. [23] (Section 3.1.2 Table 6) in the reaction scheme for both feedstocks, the model predictions for the total volatile yields agree well with the experimental results (experimental uncertainty on a 95% confidence interval). However, the char yield is slightly underpredicted (by 3.5 wt% at 600 °C) for the torrefied biomass. The model does however predict the correct trends for a change in temperature between 500 and 600 °C, and no significant deviation in char yield is observed, confirming that secondary reactions did not occur in the multi-shot pyrolyzer.

The change in the lignocellulosic composition (removal of hemicelluloses) (Table 3) was taken into account by the model; therefore, the deviation in char yield for torrefied biomass should be attributed to changes in the pyrolysis behaviour due to physico-chemical changes in the biomass structure caused by torrefaction. For example, the prior removal of water during torrefaction enhances the repolymerization reactions during subsequent pyrolysis and leads to higher char formation compared to raw biomass pyrolysis [67,68]. The experimentally observed shift in the pyrolysis reaction pathways favours char

Table 8
Details of different experimental pyrolysis reactor systems and estimated heating rates within the particles at 550 °C. Calculations at different temperatures are shown in the Supplementary Data (Section S5).

Reactor name	Pyrolysis type	Reactor diameter (mm)	Feedstock type	Feedstock particle size (μm)	Feedstock mass (mg)	Inert gas type and velocity (m/s)	Volatile residence time (s)	Pyrolysis time (min)	Internal heating rate (°C/s)	Pressure (bar)	Ref.
Multi-shot pyrolyzer	Fast	1.9	Raw wood chips	37–74	0.2	He, 0.05	1.13	1.2	110	1	
Multi-shot pyrolyzer	Fast	1.9	Torrefied wood chips	37–74	0.2	He, 0.05	1.13	1.5	110	1	
Horizontal micro-pyrolyzer	Fast	10.0	Pine sawdust	50–150	20	N_2, 0.01	7.1	1.2	27	1	[47]
High-pressure pyrolyzer	Slow	31.3	Torrefied wood chips	37–74	20 000	N_2, 0.01	19.1	82.1	0.12	1–30	[31]

Table 9
Experimental and predicted chemical composition of condensables obtained from the fast pyrolysis of raw biomass at temperatures of 500–600 °C. Values are reported in mass percentage of initial feedstock on a dry ash free basis. Experimental uncertainty based on a 95% confidence interval (Supplementary Data Section S7).

	500 °C		550 °C		600 °C	
	Exp.	Model	Exp.	Model	Exp.	Model
Volatiles	**92.0 ± 5.5**	**90.5**	**92.2 ± 5.5**	**90.5**	**92.4 ± 5.5**	**90.6**
Sugars	4.5 ± 0.3	9.0	4.7 ± 0.3	8.2	4.7 ± 0.3	7.7
Aldehydes	n.d*	6.2	n.d	6.4	n.d	6.5
Furanics	1.1 ± 0.1	2.9	1.1 ± 0.1	3.1	1.3 ± 0.1	3.1
Ketones	3.9 ± 0.2	6.0	3.6 ± 0.2	6.1	4.1 ± 0.2	6.2
Alcohols	n.d	0.7	n.d	0.6	n.d	0.6
Acids	n.d	4.2	n.d	4.3	n.d	4.4
Methoxyphenols	1.0 ± 0.1	1.1	1.0 ± 0.1	1.2	0.9 ± 0.1	1.3
Phenols	0.1 ± 0.0	0.7	0.1 ± 0.0	0.7	0.1 ± 0.0	0.8
H_2O	n.d	13.0	n.d	13.1	n.d	13.2
HMWCs	n.d	30.7	n.d	30.7	n.d	30.7
Gas	n.d	15.9	n.d	16.1	n.d	16.1
Char	**8.0 ± 0.5**	**9.5**	**7.8 ± 0.5**	**9.5**	**7.6 ± 0.5**	**9.4**

*n.d. – not determined.

production in the case of torrefied biomass (Table 10), suggesting that the kinetic parameters used to describe the char-forming reactions from cellulose and lignin, which were reported by Ranzi et al. [23] for raw biomass, cannot be applied in the case of torrefied biomass.

To improve the model for the torrefied biomass, the kinetic parameters reported by Wang et al. [58] (Section 3.1.2 Table 6) to describe the pyrolysis of the different bio-polymers in torrefied softwood were used to assess the influence of the char-forming reactions of the cellulose and lignin components (reactions 3, 10, 11 and 12). In this case, the model predictions for the char and total volatile yields are significantly improved (Table 10); confirming that pyrolysis of torrefied biomass may be described with the same semi-global lumped chemical kinetic model used for raw biomass, although different kinetic parameters should be used to describe the char-forming reactions. Furthermore, the root mean square error (RMSE) and mean absolute error (MAE) for the raw and torrefied biomass models (Table 12) were within reasonable ranges, while further demonstrating an improved fit for the case of torrefied biomass when the kinetic parameters reported by Wang et al. [58] were used.

The model outputs for the raw (Table 9) and torrefied biomass (Table 10, kinetics from Wang et al. [58]) demonstrate the important differences in the product distribution and composition for the different feedstocks. When using torrefied biomass at 600 °C, the most significant change is observed in the char yield and the model output shows a 14.6 wt% increase in comparison with the char yield from raw biomass, which agrees well with the 14.7 wt% increase shown by the experimental results. The model output also indicates that if torrefied biomass is used (at 600 °C), a 2.5 wt% decrease in the total gas yield occurs, which is attributed to greater competition between the reaction forming char (reaction 3) and those forming the intermediate compounds (reactions 4 and 5) from cellulose [25].

In the case of the condensable products, the acids significantly decrease (-3.5 wt%), ketones, aldehydes and furanics marginally decrease (-1.4, −0.8 and −0.8 wt% respectively), whereas the yields of methoxyphenols and phenols slightly increase (+1.1 and + 0.6 wt%, respectively) when torrefied biomass is used. These changes are directly related to the change in the lignocellulosic content of torrefied biomass (Table 3). The experimental results showed similar trends for the ketone groups (a decrease of 1.9 wt%) but differed for the other condensables. For example, for the sugar group, the experimental results showed that higher yields were produced when torrefied biomass instead of raw biomass was used and this has been attributed to an increase in the extent of cellulose-lignin interactions facilitating the transglycosylation of cellulose in torrefied biomass [69]. Interactions between the biopolymers were not considered in the reaction scheme, which may explain why the same trend is not predicted by the model outputs. In general, the experimental yields of the condensables for both raw and torrefied biomass are lower than those predicted by the models (Tables 9 and 10) and this may be attributed to the limited number of components detected and quantified in the Py-GC–MS/FID experimental investigation. However, the general trends in product distribution of the

Table 10
Experimental and predicted chemical composition of condensables obtained from the fast pyrolysis of torrefied biomass at temperatures of 500–600 °C. Values are reported in mass percentage of initial feedstock on a dry ash free basis. Experimental uncertainty based on a 95% confidence interval (Supplementary Data Section S7).

	500 °C			550 °C			600 °C		
	Exp.	Model (kinetics from Ranzi et al. [23])	Model (kinetics from Wang et al. [58])	Exp.	Model (kinetics from Ranzi et al. [23])	Model (kinetics from Wang et al. [58])	Exp.	Model (kinetics from Ranzi et al. [23])	Model (kinetics from Wang et al. [58])
Volatiles	78.3 ± 4.7	81.0	75.3	77.9 ± 4.7	81.1	75.7	77.7 ± 4.7	81.1	76.0
Sugars	5.7 ± 0.3	8.6	6.8	6.5 ± 0.4	7.8	6.2	6.4 ± 0.4	7.3	5.8
Aldehydes	n.d.*	6.2	5.4	n.d	6.5	5.6	n.d	6.6	5.8
Furanics	1.1 ± 0.1	2.8	2.2	1.1 ± 0.1	2.9	2.3	1.2 ± 0.1	3.0	2.3
Ketones	2.0 ± 0.1	5.9	4.7	2.9 ± 0.2	6.0	4.7	2.9 ± 0.2	6.0	4.7
Alcohols	n.d	0.9	0.8	n.d	0.9	0.6	n.d	0.8	0.6
Acids	n.d	0.9	0.8	n.d	0.9	0.8	n.d	0.9	0.8
Methoxyphenols	0.9 ± 0.1	1.5	1.9	1.1 ± 0.1	1.7	2.2	0.9 ± 0.1	1.8	2.4
Phenols	0.1 ± 0.0	0.9	1.1	0.1 ± 0.0	1.0	1.3	0.1 ± 0.0	1.0	1.4
HMWCs	n.d	28.5	24.6	n.d	28.6	24.7	n.d	28.6	24.8
H_2O	n.d	9.5	13.8	n.d	9.6	13.8	n.d	9.7	13.7
Gas	n.d	15.2	13.4	n.d	15.3	13.6	n.d	15.4	13.7
Char	21.8 ± 1.3	19.0	24.7	22.1 ± 1.3	18.9	24.3	22.3 ± 1.3	18.9	24.0

*n.d. – not determined.

condensables, predicted by the model outputs, are similar to the experimental observations. For example, the model outputs indicate that for both raw and torrefied biomass, the sugars, aldehyde and ketone groups are the major condensables, similar to what was experimentally observed (Tables 9 and 10).

4.2. Model predictions and validation of primary condensates composition

The capability of the proposed kinetic model in predicting the chemical composition of fast pyrolysis bio-oil was also evaluated in this section. The model predictions were compared to the experimental results derived from the fast pyrolysis of pine sawdust at 550 °C performed by Carrier et al. [47]. In their study, a comprehensive GC/MS analysis of the bio-oil was carried out and 97.3 % of GC peak areas were identified and quantified, corresponding to a total concentration of detected products up to 32.8 wt% in bio-oil. The full report is provided in the Supplementary Data (Section S8). A comparison of the experimental results and model predictions is shown in Table 11.

In general, the model outputs agree well with the experimental results for the yields of major pyrolysis products (volatiles and char) as well as the yields of most chemical groups in the condensates. The RMSE and MAE were within reasonable values (Table 12) and the most significant deviation between the experimental data and the model outputs was observed for the sugar group, where the experimental yields were 3.4 wt% lower than the model output. This may be attributed to the limited number of biomass-derived sugars that can be accurately detected and quantified using a single GC-column [70].

Furthermore, the reaction scheme predicts that a large fraction of the volatiles (28.6 wt%) consists of HMWCs (assumed to be representative of oligomers), which cannot directly be compared to the experimental results because the oligomer content of the bio-oil was not quantified. However, the yield of HMWCs may be validated through an indirect method. For example, the total amount of unquantified gas and condensates for the experimental data can be calculated via a mass balance, that is 41.5 wt%. Assuming that the reaction scheme predicts the correct gas yield, 15.8 wt%, the fraction of heavy condensates (GC-undetectable) can be determined as 25.7 wt%, which agrees well with the model predicted yield of the HMWCs, 28.6 wt%. Therefore, the primary reaction scheme is capable of predicting the yields for a wide range of condensate groups.

4.3. Model prediction and validation of secondary pyrolysis product composition at low pressure

The validation of the secondary reaction scheme was performed in this section by evaluating the scheme's ability to predict the yields and composition of pyrolysis products derived during slow pyrolysis of torrefied biomass in the g-scale high-pressure pyrolyzer at temperatures of 400–600 °C and 1 bar pressure. Compared to the fast pyrolysis experimental data (Sections 4.1 and 4.2), significantly higher char, gas and pyrolytic water yields were obtained in this reactor, whereas bio-oil yields were significantly lower (Fig. 3). The model outputs obtained from the joint primary and secondary reaction schemes correspond well to these trends.

The RMSE and MAE were similar to the values obtained for the validation of the primary scheme and within acceptable ranges (Table 14). The largest deviations between model outputs and experimental data for the major pyrolysis products (char, gas, bio-oil, and pyrolytic water) were observed for the gas and char yields at 400 °C: Char yields were under-predicted by 3.4 wt%, whereas gas yields were over-predicted by 3.4 wt% (Fig. 3). These deviations are no longer evident at 500 °C, suggesting that, in this reactor, charring reaction pathways are favoured against volatilization pathways at lower temperatures, which was described in the reaction scheme (the competition between reactions 1, 2 and reaction 3 for cellulose decomposition). However, compared to the experimental data, the effects of those competing reactions were not as significant in the model outputs.

Comparing the individual gas species, the major gases were CO and CO_2 and the CO yields were slightly under-predicted by around 2.0 wt% at temperatures above 550 °C (Fig. 4), which could be due to the increased catalytic effect of inherent inorganics in torrefied biomass on cracking reactions [65,71], which become more significant at higher temperatures but were not considered in the reaction scheme. The yields of the minor gases CH_4 and H_2 were over-predicted (Fig. 4), possibly due to their retention in the char, which was not accounted for [25].

Table 11
Experimental and predicted chemical composition of condensates from the fast pyrolysis of pine sawdust at 550 °C. Values are reported in mass percentage of initial feedstock on a dry ash free basis.

	Exp.	Model
Volatiles	**80.3 ± 1.8**	**80.8**
Sugars	4.6 ± 0.1	8.0
Aldehydes	6.1 ± 0.1	5.9
Furanics	2.2 ± 0.1	2.4
Ketones	7.9 ± 0.2	5.4
Alcohols	0.4 ± 0.0	1.0
Acids	4.6 ± 0.1	1.6
Methoxyphenols	1.3 ± 0.0	1.7
Phenols	0.7 ± 0.0	1.0
HMWCs	n.d.	28.6
H_2O	12.7 ± 0.3	9.5
Gas	n.d.	15.8
Unquantified gas and condensates	41.5	n.d.
Char	**19.7 ± 0.5**	**19.2**

*n.d. – not determined.

Table 12
Statistical performance parameters for μg- and mg-scale micropyrolyzer kinetic models.

Pyrolysis reactor	Kinetic data source	Feedstock	RMSE	MAE
μg-scale micropyrolyzer (Multi-shot pyrolyzer)	Ranzi et al. [23]	Raw biomass	1.9	1.5
μg-scale micropyrolyzer (Multi-shot pyrolyzer)	Ranzi et al. [23]	Torrefied biomass	2.0	1.6
μg-scale micropyrolyzer (Multi-shot pyrolyzer)	Wang et al. [58]	Torrefied biomass	1.5	1.2
mg-scale micropyrolyser (Horizontal pyrolyzer)	Ranzi et al. [23]	Raw biomass	1.7	1.2

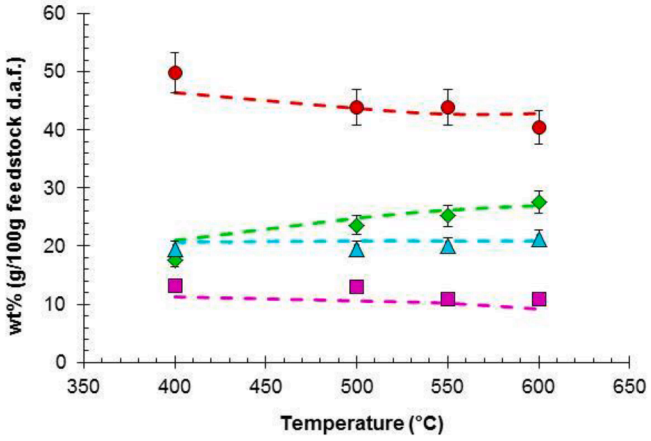

Fig. 3. Comparison of experimental results and model predictions for slow pyrolysis of torrefied biomass in a fixed bed reactor at 1 bar. Char yield: Experimental data (●), model prediction (—), gas yield: Experimental data (◆), model prediction (—), water yield: Experimental data (▲), model prediction (—) and bio-oil yield: Experimental data (■), model prediction (—).

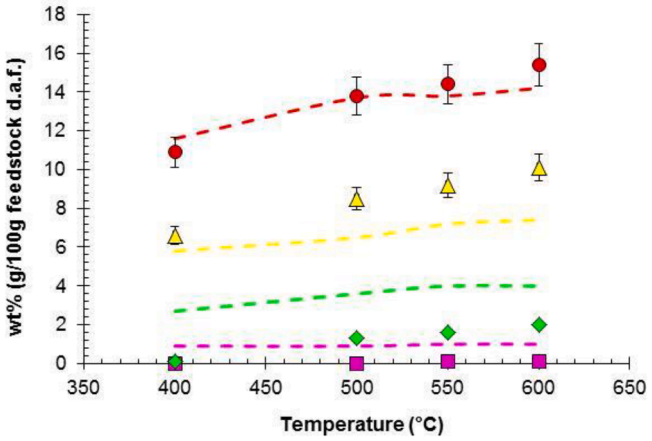

Fig. 4. Comparison of experimental results and model predictions for slow pyrolysis of torrefied biomass in a fixed bed reactor at 1 bar. CO_2 yield: Experimental data (●), model prediction (▬), CO yield: Experimental data (△), model prediction (▬), CH_4 yield: Experimental data (◆), model prediction (▬) and H_2 yield: Experimental data (■), model prediction (▬).

In the case of the bio-oil yield (Fig. 3), the model outputs agree well with the experimental data, with both indicating a decrease in yield of around 2.0 wt% for a temperature increase from 400 to 600 °C; confirming the significant extent of secondary reactions at these temperatures in the reactor. The pyrolytic water yields were also well predicted by the reaction scheme for the entire temperature range (Fig. 3). The reaction scheme's ability to predict the composition of the bio-oil was difficult to critically evaluate due to the large number of GC-undetected products (Table 13). In general, the predicted yields of the condensate groups were significantly lower compared to the yields obtained in the fast pyrolysis reactors (Sections 4.1 and 4.2), which agrees with the experimental observations and is attributed to the low heating rate (7 °C/min) used in the reactor that would favour rearrangement/primary charring over fragmentation pathways [28]. The yield of the sugar group (Table 13) decreased most significantly and this trend was well predicted by the reaction scheme, which also allowed for the decomposition of the primary sugars into secondary products. Another significant difference in the predicted bio-oil composition was that the large yields of HMWCs derived in the fast pyrolysis reactors (Sections 4.1 and 4.2) were absent due to their conversion into secondary char, water and non-condensable gases. However, this could not be verified from the experimental data, which did not report on the content of oligomers in the bio-oil.

Table 14
Statistical performance parameters for fixed bed reactor kinetic models at different pressures.

Pyrolysis pressure (bar)	RMSE	MAE
1	1.8	1.4
15	1.5	1.1
30	1.5	1.1

4.4. Model prediction and validation of secondary pyrolysis product composition at high pressures

The validation of the reaction scheme at intermediate (15 bar) and high (30 bar) pressures is performed in this section for a temperature range of 400–600 °C. Compared with the low pressure statistical performance parameters, the RMSE and MAE were improved at the higher pressures (Table 14), indicating the model's capability of describing high pressure pyrolysis. In the experimental work of Gouws et al. [31], the pressure showed the most significant effect on the bio-oil yields, which decreased by 6.9 wt% for a pressure increase of 1 to 15 bar at 600 °C. Moreover, the effect of pressure was most significant in the range of 1–15 bar and the bio-oil yield decreased by only a further 0.8 wt % with an increase in pressure from 15 to 30 bar. The model outputs agree well with these experimental trends (Fig. 5), predicting a 5.4 wt% decrease in bio-oil yield for a pressure increase from 1 to 15 bar at 600 °C, and a 0.2 wt% decrease between 15 and 30 bar. Wafiq et al. [72] explained the small change in bio-oil yield between intermediate and high pressures from a transport perspective by suggesting counteracting effects between the diffusion of volatiles out of the pyrolyzing particle and enhanced thermal cracking with an increase in pressure. In the secondary reaction scheme proposed here, this phenomenon is explained chemically by the assumption that the gas-phase secondary reactions rates are a function of the primary volatiles partial pressure; therefore, these primary volatiles are converted to a greater extent with increasing pressure. At 1 bar, the ketone and aldehyde groups are still dominant in the bio-oil (Table 13) but at 15 bar they are almost fully converted to secondary products (Table 15). Therefore, a further increase in pressure to 30 bar does not show the same significant effect on the total bio-oil yield as was the case when increasing the pressure between 1 and 15 bar (Table 16). Furthermore, the composition of the bio-oil is well-predicted by the reaction scheme for the sugar, methoxyphenol and acid groups at 15 and 30 bar (Tables 15 and 16). The experimental data showed a significant decrease in the yield of sugars in bio-oil with an increase in pressure, with no sugar groups detected in the bio-oil above 500 °C for pressures of 15 and 30 bar. These trends were well-described by the reaction scheme, showing that the sugar groups are fully converted to secondary products (char and non-condensable gases) at high pressures.

The total gas and char yields were also well-predicted by the

Table 13
Comparison of experimental results and model predictions for bio-oil composition during slow pyrolysis of torrefied biomass in a fixed bed reactor at 400–600 °C and 1 bar. Values reported in mass percentage of initial feedstock on a dry ash free basis.

	400 °C		500 °C		550 °C		600 °C	
	Exp.	Model	Exp.	Model	Exp.	Model	Exp.	Model
Total bio-oil	13.1 ± 0.9	11.3	13.0 ± 0.9	10.6	10.9 ± 0.8	10.2	10.8 ± 0.8	9.2
Sugars	0.4 ± 0.0	0.5	0.5 ± 0.0	0.0	0.4 ± 0.0	0.0	0.3 ± 0.0	0.0
Aldehydes	0.0 ± 0.0	3.5	0.0 ± 0.0	3.4	0.0 ± 0.0	3.2	0.0 ± 0.0	2.7
Furanics	0.2 ± 0.0	1.2	0.4 ± 0.0	1.2	0.3 ± 0.0	1.2	0.2 ± 0.0	1.2
Ketones	0.0 ± 0.0	3.9	0.1 ± 0.0	3.8	0.0 ± 0.0	3.6	0.1 ± 0.0	3.0
Alcohols	0.0 ± 0.0	1.5	0.0 ± 0.0	1.5	0.0 ± 0.0	1.5	0.0 ± 0.0	1.6
Acids	0.4 ± 0.0	0.4	0.4 ± 0.0	0.4	0.6 ± 0.0	0.4	0.6 ± 0.0	0.4
Methoxyphenols	0.5 ± 0.0	0.2	0.7 ± 0.0	0.2	0.7 ± 0.0	0.2	0.7 ± 0.0	0.2
Phenols	0.0 ± 0.0	0.1	0.0 ± 0.0	0.1	0.0 ± 0.0	0.1	0.1 ± 0.0	0.1
HMWCs	n.d.*	0.0	n.d.*	0.0	n.d.*	0.0	n.d.*	0.0
GC-undetected	11.5 ± 0.8	n.d.*	11.0 ± 0.8	n.d.*	8.9 ± 0.6	n.d.*	8.7 ± 0.6	n.d.*

*n.d. – not determined.

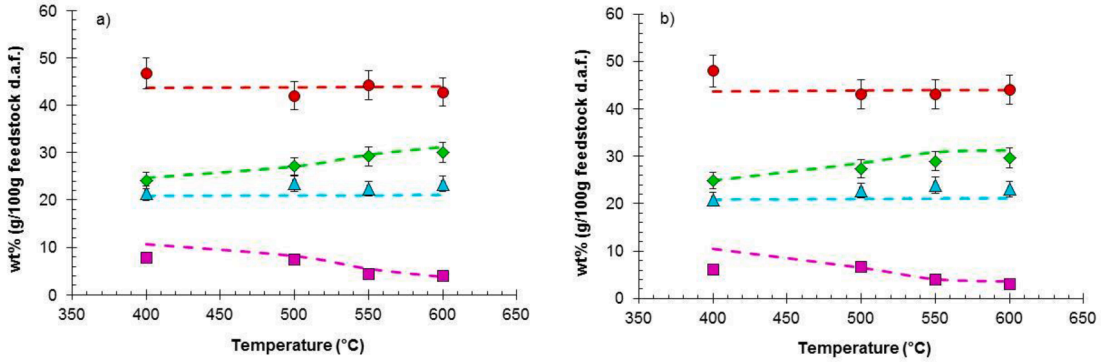

Fig. 5. Comparison of experimental results and model predictions for slow pyrolysis of torrefied biomass in a fixed bed reactor at a) 15 bar and b) 30 bar. Char yield: Experimental data (●), model prediction (—), gas yield: Experimental data (◆), model prediction (– –), water yield: Experimental data (▲), model prediction (– –) and bio-oil yield: Experimental data (■), model prediction (—).

Table 15
Comparison of experimental results and model predictions for bio-oil composition during slow pyrolysis of torrefied biomass in a fixed bed reactor at 15 bar for temperatures of 400–600 °C. Values reported in mass percentage of initial feedstock on a dry ash free basis.

	400 °C		500 °C		550 °C		600 °C	
	Exp.	Model	Exp.	Model	Exp.	Model	Exp.	Model
Total oil	7.8 ± 0.5	10.7	7.5 ± 0.5	8.2	4.3 ± 0.3	5.5	3.9 ± 0.3	3.8
Sugars	0.1 ± 0.0	0.0	0.0 ± 0.0	0.0	0.0 ± 0.0	0.0	0.0 ± 0.0	0.0
Aldehydes	0.0 ± 0.0	3.4	0.0 ± 0.0	2.2	0.0 ± 0.0	0.9	0.0 ± 0.0	0.1
Furanics	0.0 ± 0.0	1.2	0.1 ± 0.0	1.2	0.1 ± 0.0	1.2	0.1 ± 0.0	1.2
Ketones	0.0 ± 0.0	3.8	0.0 ± 0.0	2.5	0.0 ± 0.0	1.0	0.0 ± 0.0	0.1
Alcohols	0.0 ± 0.0	1.5	0.0 ± 0.0	1.6	0.0 ± 0.0	1.6	0.0 ± 0.0	1.6
Acids	0.2 ± 0.0	0.4	0.3 ± 0.0	0.4	0.3 ± 0.0	0.4	0.3 ± 0.0	0.4
Methoxyphenols	0.5 ± 0.0	0.2	0.3 ± 0.0	0.2	0.2 ± 0.0	0.2	0.2 ± 0.0	0.2
Phenols	0.0 ± 0.0	0.1	0.0 ± 0.0	0.1	0.0 ± 0.0	0.1	0.1 ± 0.0	0.1
HMWCs	0.0 ± 0.0	0.0	0.0 ± 0.0	0.0	0.0 ± 0.0	0.0	0.0 ± 0.0	0.0
GC-undetected	7.0 ± 0.5	n.d.*	6.6 ± 0.5	n.d.*	3.6 ± 0.3	n.d.*	3.2 ± 0.2	n.d.*

*n.d. – not determined

Table 16
Comparison of experimental results and model predictions for bio-oil composition during slow pyrolysis of torrefied biomass in a fixed bed reactor at 30 bar for temperatures of 400–600 °C. Values reported in mass percentage of initial feedstock on a dry ash free basis.

	400 °C		500 °C		550 °C		600 °C	
	Exp.	Model	Exp.	Model	Exp.	Model	Exp.	Model
Total oil	6.1 ± 0.4	10.5	6.7 ± 0.5	6.5	3.9 ± 0.3	4.1	3.1 ± 0.2	3.6
Sugars	0.1 ± 0.0	0.0	0.0 ± 0.0	0.0	0.0 ± 0.0	0.0	0.0 ± 0.0	0.0
Aldehydes	0.0 ± 0.0	3.3	0.0 ± 0.0	1.4	0.0 ± 0.0	0.2	0.0 ± 0.0	0.0
Furanics	0.0 ± 0.0	1.2	0.1 ± 0.0	1.2	0.1 ± 0.0	1.2	0.0 ± 0.0	1.2
Ketones	0.0 ± 0.0	3.7	0.0 ± 0.0	1.6	0.0 ± 0.0	0.3	0.0 ± 0.0	0.0
Alcohols	0.0 ± 0.0	1.5	0.0 ± 0.0	1.6	0.0 ± 0.0	1.6	0.0 ± 0.0	1.6
Acids	0.3 ± 0.0	0.4	0.3 ± 0.0	0.4	0.3 ± 0.0	0.4	0.3 ± 0.0	0.4
Methoxyphenols	0.4 ± 0.0	0.2	0.3 ± 0.0	0.2	0.2 ± 0.0	0.2	0.1 ± 0.0	0.2
Phenols	0.0 ± 0.0	0.1	0.0 ± 0.0	0.1	0.1 ± 0.0	0.1	0.1 ± 0.0	0.1
HMWCs	0.0 ± 0.0	0.0	0.0 ± 0.0	0.0	0.0 ± 0.0	0.0	0.0 ± 0.0	0.0
GC-undetected	5.3 ± 0.4	n.d.*	6.1 ± 0.4	n.d.*	3.3 ± 0.2	n.d.*	2.5 ± 0.2	n.d.*

*n.d. – not determined.

proposed reaction scheme, with the char yield showing a slight increase in the range of 1 to 15 bar (Figs. 3 and 5a) and no significant change in the range from 15 to 30 bar (Fig. 5a-b), whereas the gas yields increased significantly between 1 and 15 bar (Figs. 3 and 5a) but also showed a less significant change for 15 to 30 bar (Fig. 5a-b). Comparing the yields of individual non-condensable gases (Fig. 6), the CO yield was well-predicted, whereas the CO_2 yield was slightly under-predicted. The CH_4 and H_2 yields were over-predicted, possibly due to their retention in the char [25]. However, the reaction scheme well-described the overall trend of the H_2 yield, which increased significantly with pressure for the range of 1 to 15 bar (Figs. 4 and 6a), attributed to the increase in extent of secondary reactions with pressure [31,72].

5. Practical implications

The accurate and robust modelling of the pyrolysis process is an important requirement for improving reactor efficiency and controllability in order to maximize profitability. Although various pyrolysis models are available (Table 1), the use of these models is, in most cases, limited to the conditions and fuels for which they were developed and

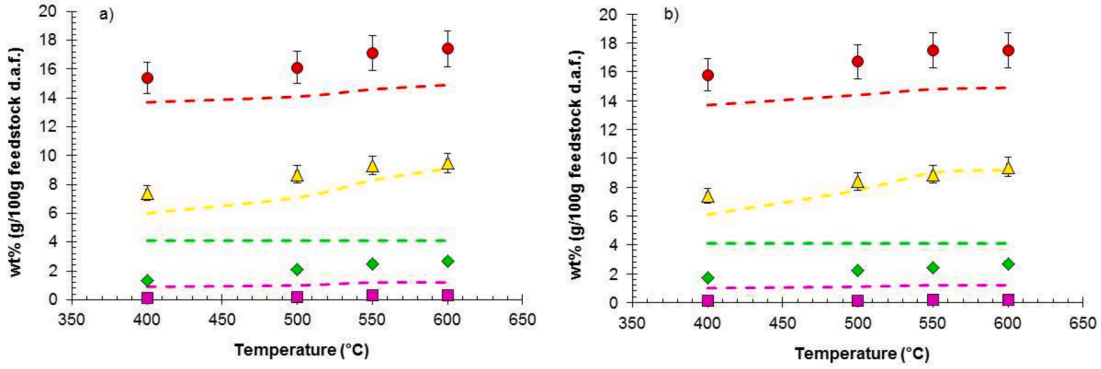

Fig. 6. Comparison of experimental results and model predictions for slow pyrolysis of torrefied biomass in a fixed bed reactor at a) 15 bar and b) 30 bar. CO_2 yield: Experimental data (●), model prediction (—), CO yield: Experimental data (△), model prediction (—), CH_4 yield: Experimental data (◆), model prediction (—) and H_2 yield: Experimental data (■), model prediction (—).

only applicable to laboratory scale reactors, limiting their practical application to real-world commercial reactors. Due to the adjustable nature of the proposed lumped kinetic model, the model is able to well-predict the pyrolysis product yields and composition for different scales of pyrolysis reactors. Furthermore, the model takes into consideration the effect of pressure, which is significant in commercial high pressure gasifiers. In comparison to existing pyrolysis models, the proposed model may therefore be of greater practical use in real-world reactors.

6. Conclusion and future perspectives

A new semi-global kinetic model that may be applied to different scales of pyrolysis reactors (with a wide range of operating conditions) was proposed here for the pyrolysis of raw and torrefied biomass. The model was based on an adjustable mechanistic reaction scheme where the lignocellulosic composition was used as an input parameter (thereby accounting for compositional differences between raw and torrefied biomass), and the primary/secondary reactions presence were varied based on the main process characteristics of the pyrolysis reactor (heating rate, temperature, volatile residence time and pressure).

The primary reaction scheme was validated by comparing the model outputs with the experimental yields of condensables and condensates derived in two different micropyrolyzers (μg- and mg-scale respectively). In general, the comparison was satisfactory, with the model predicting the correct trends when torrefied instead of raw biomass was used in the μg-scale pyrolyzer: increased char yields and decreased acid yields. The reliability of the model was further proven by its accuracy in predicting the yields of a range of chemical condensate groups (maximum deviation $<$ 4 wt%) in bio-oil derived in a mg-scale micropyrolyzer.

The secondary reaction scheme was validated through comparison with experimental data derived in a g-scale fixed bed reactor (long vapour residence time, low heating rate) at both low and high pressures. In general, the model showed reasonable accuracy when predicting the yields and composition of the pyrolysis products: bio-oil yields significantly decreased in the range of 1–15 bar, whereas gas yields increased. Moreover, the composition of the bio-oil and gas was changed: sugar groups were absent at higher pressures, whereas CO_2 and H_2 yields increased. The changes in product distribution between 15 and 30 bar were less significant and this was well-described by the model through the assumption that the secondary gas-phase reaction rates were a function of the primary volatiles partial pressure.

The limitations of the model (Table 1) include its inability to account for the catalytic effects of inherent inorganics as well as the interactions between biomass components. Furthermore, the reactions forming the intermediate LMWCs cannot be directly verified through experimental data and more precise kinetic parameters are required for the specific secondary liquid- and gas-phase reactions. Future work should focus on further validating the reaction scheme, specifically at temperatures below 400 °C and above 600 °C, using comprehensive data on bio-oil composition. The determination of more precise kinetic parameters for the secondary decomposition of HMWCs in bio-oil may also improve the accuracy of the model. Moreover, the rigor of those kinetic parameters should be verified. Furthermore, the interaction between biopolymers and the catalytic effects of inherent inorganics may also be added to expand the reaction scheme for a wider range of raw/torrefied biomasses. The model should also be validated for commercial scale pyrolysis reactors.

Declaration of Competing Interest

The authors declare that they have no known competing financial interests or personal relationships that could have appeared to influence the work reported in this paper.

Acknowledgements

The authors gratefully acknowledge Justine Arocas for technical assistance with the py-GC/MS/FID equipment. The authors also acknowledge the French scientific program MOPGA (reference ANR-18-MPGA-0013) managed by the National Research Agency and financially supported by the "Investissements d'Avenir" and Region Occitanie (18016004).

This work was financially supported by the National Research Foundation (NRF), South Africa [Coal Research Chair Grant No. 86880] and Sasol. Opinions, findings and conclusions or recommendations expressed in any publication generated by the NRF supported research are that of the author(s) alone, and that the NRF accepts no liability whatsoever in this regard.

Appendix A. Supplementary data

Supplementary data to this article can be found online at https://doi.org/10.1016/j.enconman.2021.115199.

References

[1] U.S.E.I. Administration. International Energy Outlook 2017. https://www.eia.gov/outlooks/ieo/pdf/0484(2017).pdf. Accessed 19 March 2018.
[2] I.E. Agency. World Energy Outlook 2019. https://www.iea.org/reports/world-energy-outlook-2019. Accessed 31 March 2020.

[3] Bridgwater A, Peacocke G. Fast pyrolysis processes for biomass. Renew Sustain Energy Rev 2000;4:1–73.
[4] Van de Beld B, Holle E, Florijn J. The use of pyrolysis oil and pyrolysis oil derived fuels in diesel engines for CHP applications. Appl Energy 2013;102:190–7.
[5] Bridgwater A. The production of biofuels and renewable chemicals by fast pyrolysis of biomass. Int J Global Energy Issues 2007;27:160–203.
[6] Meng J, Park J, Tilotta D, Park S. The effect of torrefaction on the chemistry of fast-pyrolysis bio-oil. Bioresour Technol 2012;111:439–46.
[7] Ji-lu Z. Bio-oil from fast pyrolysis of rice husk: Yields and related properties and improvement of the pyrolysis system. J Anal Appl Pyrol 2007;80(1):30–5.
[8] Acharya B, Sule I, Dutta A. A review on advances of torrefaction technologies for biomass processing. Biomass Convers Biorefin 2012;2(4):349–69.
[9] Adams P, Shirley J, McManus M. Comparative cradle-to-gate life cycle assessment of wood pellet production with torrefaction. Appl Energy 2015;138:367–80.
[10] Phanphanich M, Mani S. Impact of torrefaction on the grindability and fuel characteristics of forest biomass. Bioresour Technol 2011;102:1246–53.
[11] Chew J, Doshi V. Recent advances in biomass pretreatment–Torrefaction fundamentals and technology. Renew Sustain Energy Rev 2011;15:4212–22.
[12] White JE, Catallo WJ, Legendre BL. Biomass pyrolysis kinetics: a comparative critical review with relevant agricultural residue case studies. J Anal Appl Pyrol 2011;91:1–33.
[13] Sharifzadeh M, Sadeqzadeh M, Guo M, Borhani TN, Konda NM, Garcia MC, et al. The multi-scale challenges of biomass fast pyrolysis and bio-oil upgrading: Review of the state of art and future research directions. Prog Energy Combust Sci 2019;71:1–80.
[14] Xia C, Cai L, Zhang H, Zuo L, Shi SQ, Lam SS. A review on the modeling and validation of biomass pyrolysis with a focus on product yield and composition. Biofuel Res J 2021;8:2292–8782.
[15] Perera SM, Wickramasinghe C, Samarasiri B, Narayana M. Modeling of thermochemical conversion of waste biomass–a comprehensive review. Biofuel Res J 2021;8:1481–528.
[16] Antal MJJ, Varhegyi G. Cellulose pyrolysis kinetics: the current state of knowledge. Ind Eng Chem Res 1995;34(3):703–17.
[17] Shafizadeh F. Introduction to pyrolysis of biomass. J Anal Appl Pyrol 1982;3:283–305.
[18] Di Blasi C, Lanzetta M. Intrinsic kinetics of isothermal xylan degradation in inert atmosphere. J Anal Appl Pyrol 1997;40:287–303.
[19] Mamleev V, Bourbigot S, Le Bras M, Yvon J. The facts and hypotheses relating to the phenomenological model of cellulose pyrolysis: Interdependence of the steps. J Anal Appl Pyrol 2009;84(1):1–17.
[20] Rousset P, Turner I, Donnot A, Perré P. The choice of a low-temperature pyrolysis model at the microscopic level for use in a macroscopic formulation. Annals of Forest Science. 2006;63:213–29.
[21] Carstensen H-H, Dean AM. Rate constant rules for the automated generation of gas-phase reaction mechanisms. The Journal of Physical Chemistry A. 2009;113:367–80.
[22] Vikram S, Rosha P, Kumar S. Recent Modeling Approaches to Biomass Pyrolysis: A Review. Energy Fuels 2021;35(9):7406–33.
[23] Ranzi E, Debiagi PEA, Frassoldati A. Mathematical modeling of fast biomass pyrolysis and bio-oil formation. Note I: Kinetic mechanism of biomass pyrolysis. ACS Sustainable Chem Eng 2017;5(4):2867–81.
[24] Van Dyk J, Keyser M, Coertzen M. Syngas production from South African coal sources using Sasol-Lurgi gasifiers. Int J Coal Geol 2006;65:243–53.
[25] Anca-Couce A, Mehrabian R, Scharler R, Obernberger I. Kinetic scheme of biomass pyrolysis considering secondary charring reactions. Energy Convers Manage 2014;87:687–96.
[26] Ranzi E, Cuoci A, Faravelli T, Frassoldati A, Migliavacca G, Pierucci S, et al. Chemical kinetics of biomass pyrolysis. Energy Fuels 2008;22:4292–300.
[27] Bridgwater A. Principles and practice of biomass fast pyrolysis processes for liquids. J Anal Appl Pyrol 1999;51:3–22.
[28] Collard F-X, Blin J. A review on pyrolysis of biomass constituents: Mechanisms and composition of the products obtained from the conversion of cellulose, hemicelluloses and lignin. Renew Sustain Energy Rev 2014;38:594–608.
[29] Onay O, Kockar OM. Slow, fast and flash pyrolysis of rapeseed. Renewable Energy 2003;28:2417–33.
[30] Bridgwater A, Meier D, Radlein D. An overview of fast pyrolysis of biomass. Org Geochem 1999;30:1479–93.
[31] Gouws SM, Carrier M, Bunt JR, Neomagus HWJP. Co-pyrolysis of torrefied biomass and coal: Effect of pressure on synergistic reactions. J Anal Appl Pyrol 2022;161:105363. https://doi.org/10.1016/j.jaap.2021.105363.
[32] Azeez AM, Meier D, J.r. Odermatt, T. Willner. Fast pyrolysis of African and European lignocellulosic biomasses using Py-GC/MS and fluidized bed reactor. Energy Fuels 2010;24:2078–85.
[33] Neupane S, Adhikari S, Wang Z, Ragauskas AJ, Pu Y. Effect of torrefaction on biomass structure and hydrocarbon production from fast pyrolysis. Green Chem 2015;17:2406–17.
[34] Cai W, Liu Q, Shen D, Wang J. Py-GC/MS analysis on product distribution of two-staged biomass pyrolysis. J Anal Appl Pyrol 2019;138:62–9.
[35] Chen D, Zhou J, Zhang Q. Effects of torrefaction on the pyrolysis behavior and bio-oil properties of rice husk by using TG-FTIR and Py-GC/MS. Energy Fuels 2014;28:5857–63.
[36] Adhikari S, Srinivasan V, Fasina O. Catalytic pyrolysis of raw and thermally treated lignin using different acidic zeolites. Energy Fuels 2014;28:4532–8.
[37] Ben H, Ragauskas AJ. Torrefaction of Loblolly pine. Green Chem 2012;14:72–6.
[38] Akalın MK, Karagöz S. Analytical pyrolysis of biomass using gas chromatography coupled to mass spectrometry. TrAC, Trends Anal Chem 2014;61:11–6.
[39] Stark SM, Neurock M, Klein MT. Strategies for modelling kinetic interactions in complex mixtures: Monte Carlo algorithms for MIMD parallel architectures. Chem Eng Sci 1993;48:4081–96.
[40] Sunphorka S, Chalermsinsuwan B, Piumsomboon P. Artificial neural network model for the prediction of kinetic parameters of biomass pyrolysis from its constituents. Fuel 2017;193:142–58.
[41] Aghbashlo M, Tabatabaei M, Nadian MH, Davoodnia V, Soltanian S. Prognostication of lignocellulosic biomass pyrolysis behavior using ANFIS model tuned by PSO algorithm. Fuel 2019;253:189–98.
[42] Aghbashlo M, Almasi F, Jafari A, Nadian MH, Soltanian S, Lam SS, et al. Describing biomass pyrolysis kinetics using a generic hybrid intelligent model: A critical stage in sustainable waste-oriented biorefineries. Renewable Energy 2021;170:81–91.
[43] Sheng C, Azevedo J. Modeling biomass devolatilization using the chemical percolation devolatilization model for the main components. Proc Combust Inst 2002;29:407–14.
[44] Niksa S. Predicting the rapid devolatilization of diverse forms of biomass with bio-flashchain. Proc Combust Inst 2000;28:2727–33.
[45] Chen Y, Charpenay S, Jensen A, Wójtowicz MA, Serio MA. Modeling of biomass pyrolysis kinetics. Symp (Int) Combust 1998;27(1):1327–34.
[46] Moore A, Park S, Segura C, Carrier M. Fast pyrolysis of lignin-coated radiata pine. J Anal Appl Pyrol 2015;115:203–13.
[47] Carrier M, Windt M, Ziegler B, Appelt J, Saake B, Meier D, et al. Quantitative insights into the fast pyrolysis of extracted cellulose, hemicelluloses, and lignin. ChemSusChem 2017;10(16):3212–24.
[48] Ranzi E, Debiagi PEA, Frassoldati A. Mathematical modeling of fast biomass pyrolysis and bio-oil formation. Note II: secondary gas-phase reactions and bio-oil formation. ACS Sustainable Chem Eng 2017;5:2882–96.
[49] Anca-Couce A. Reaction mechanisms and multi-scale modelling of lignocellulosic biomass pyrolysis. Prog Energy Combust Sci 2016;53:41–79.
[50] Zhou S, Pecha B, van Kuppevelt M, McDonald AG, Garcia-Perez M. Slow and fast pyrolysis of Douglas-fir lignin: Importance of liquid-intermediate formation on the distribution of products. Biomass Bioenergy 2014;66:398–409.
[51] Piskorz J, Radlein DSA, Scott DS, Czernik S. Pretreatment of wood and cellulose for production of sugars by fast pyrolysis. J Anal Appl Pyrol 1989;16:127–42.
[52] Anca-Couce A, Obernberger I. Application of a detailed biomass pyrolysis kinetic scheme to hardwood and softwood torrefaction. Fuel 2016;167:158–67.
[53] Dufour A, Ouartassi B, Bounaceur R, Zoulalian A. Modelling intra-particle phenomena of biomass pyrolysis. Chem Eng Res Des 2011;89:2136–46.
[54] Xiong Z, Guo J, Chaiwat W, Deng W, Hu X, Han H, et al. Assessing the chemical composition of heavy components in bio-oils from the pyrolysis of cellulose, hemicellulose and lignin at slow and fast heating rates. Fuel Process Technol 2020;199:106299.
[55] Smith MW, Pecha B, Helms G, Scudiero L, Garcia-Perez M. Chemical and morphological evaluation of chars produced from primary biomass constituents: Cellulose, xylan, and lignin. Biomass Bioenergy 2017;104:17–35.
[56] Montoya J, Pecha B, Janna FC, Garcia-Perez M. Single particle model for biomass pyrolysis with bubble formation dynamics inside the liquid intermediate and its contribution to aerosol formation by thermal ejection. J Anal Appl Pyrol 2017;124:204–18.
[57] Vinu R, Broadbelt LJ. A mechanistic model of fast pyrolysis of glucose-based carbohydrates to predict bio-oil composition. Energy Environ Sci 2012;5:9808–26.
[58] Wang S, Ru B, Dai G, Lin H, Zhang L. Influence mechanism of torrefaction on softwood pyrolysis based on structural analysis and kinetic modeling. Int J Hydrogen Energy 2016;41:16428–35.
[59] Di Blasi C. Numerical simulation of cellulose pyrolysis. Biomass Bioenergy 1994;7:87–98.
[60] Branca C, Di Blasi C, Elefante R. Devolatilization of conventional pyrolysis oils generated from biomass and cellulose. Energy Fuels 2006;20:2253–61.
[61] Park WC, Atreya A, Baum HR. Experimental and theoretical investigation of heat and mass transfer processes during wood pyrolysis. Combust Flame 2010;157:481–94.
[62] Ahuja P, Kumar S, Singh PC. A model for primary and heterogeneous secondary reactions of wood pyrolysis. Chemical Eng Technol: Indust Chem-Plant Equip-Process Eng-Biotechnol 1996;19:272–82.
[63] Morf P, Hasler P, Nussbaumer T. Mechanisms and kinetics of homogeneous secondary reactions of tar from continuous pyrolysis of wood chips. Fuel 2002;81:843–53.
[64] Anca-Couce AS, Dieguez-Alonso A, Zobel N, Berger A, Kienzl N, Behrendt F. Influence of heterogeneous secondary reactions during slow pyrolysis on char oxidation reactivity of woody biomass. Energy Fuels 2017;31:2335–44.
[65] Hoekstra E, Westerhof RJ, Brilman W, Van Swaaij WP, Kersten SR, Hogendoorn KJ, et al. Heterogeneous and homogeneous reactions of pyrolysis vapors from pine wood. AIChE J 2012;58:2830–42.
[66] Jones JR, Chen Q, Ripberger GD. Secondary reactions and the heat of pyrolysis of wood. Energy Technology. 2020;8:1–13.
[67] Wannapeera J, Fungtammasan B, Worasuwannarak N. Effects of temperature and holding time during torrefaction on the pyrolysis behaviors of woody biomass. J Anal Appl Pyrol 2011;92:99–105.
[68] Shen D. The pyrolytic mechanism of the main components in woody biomass and their interactions. University of Southampton: Faculty of Engineering, Science and Mathematics; 2011.
[69] Hosoya T, Kawamoto H, Saka S. Solid/liquid-and vapor-phase interactions between cellulose-and lignin-derived pyrolysis products. J Anal Appl Pyrol 2009;85:237–46.

[70] Michailof CM, Kalogiannis KG, Sfetsas T, Patiaka DT, Lappas AA. Advanced analytical techniques for bio-oil characterization. Wiley Interdiscip Rev: Energy Environ 2016;5:614–39.
[71] Gouws SM, Carrier M, Bunt JR, Neomagus HWJP. Co-pyrolysis of coal and raw/torrefied biomass: A review on chemistry, kinetics and implementation. Renew Sustain Energy Rev 2021;135:110189. https://doi.org/10.1016/j.rser.2020.110189.
[72] Wafiq A, Reichel D, Hanafy M. Pressure influence on pyrolysis product properties of raw and torrefied Miscanthus: Role of particle structure. Fuel 2016;179:156–67.